Structural Role of Fluoride in the Ion-Conducting Glass System B₂O₃−PbO−LiF Studied by Single- and Double-Resonance NMR

A. S. Cattaneo,[†,‡] R. P. Lima,[§] C. E. Tambelli,[§] C. J. Magon,[§] V. R. Mastelaro,[§] A. Garcia,[§] J. E. de Souza,[§] A. S. S. de Camargo,[§] C. C. de Araujo,[†] J. F. Schneider,[§] J. P. Donoso,[§] and H. Eckert*,[†]

Institut für Physikalische Chemie, Westfälische Wilhelms−Universität Münster, Corrensstrasse 30, D-48149 Münster, Germany, Dipartimento di Scienza dei Materiali, Università degli Studi di Milano-Bicocca, Via R. Cozzi 53, I-20125 Milano, Italy, and Instituto de Fisica de São Carlos, Universidade de São Paulo, Av. Trabalhador São-carlense 400, São Carlos, SP, CEP 13566-590, Brazil

The local structure of an ion-conducting glass with nominal composition 50B₂O₃−10PbO−40LiF has been investigated by complementary ⁷Li, ¹¹B, ¹⁹F, and ²⁰⁷Pb single- and double-resonance experiments. The results give insight into the structural role of the lithium fluoride additive in borate glasses: (1) LiF is seen to actively participate in the network transformation process contributing to the conversion of three- into four-coordinate boron units, as shown by ¹¹B single-resonance as well as by ¹¹B{¹⁹F} and ¹⁹F{¹¹B} double-resonance experiments. (2) ¹⁹F signal quantification experiments suggest substantial fluoride loss, presumably caused by formation of volatile BF₃. A part of the fluoride remains in the dopant role, possibly in the form of small LiF-like cluster domains, which serve as a mobile ion supply. (3) The extent of lithium−fluorine and lead−fluorine interactions has been characterized by ⁷Li{¹⁹F} and ²⁰⁷Pb{¹⁹F} REDOR and SEDOR experiments. On the basis of these results, a quantitative structural description of this system has been developed.

Introduction

Fast-ion conducting (FIC) glasses have received much attention because of their potential application as solid electrolytes in electrochemical devices.[1–6] Glasses formed by B₂O₃, a network modifier (such as Li₂O), and a metal halide (LiCl or LiF) are representative of a class of FIC glasses in which the lithium ions are highly mobile below the glass transition temperature. Ionic conductivities between 10^{-3} and 10^{-4} S/cm at room temperature have been reported.[2,7] In addition, lead fluoroborate glasses are interesting host materials for luminescent rare-earth ions for potential laser applications.[8,9] In an effort of optimizing physical properties, the local structure and dynamics of lithium borate based glasses have been extensively investigated by experimental techniques and molecular dynamic simulations.[10–14] Nuclear Magnetic Resonance (NMR) has proven to be a powerful tool in the study of local structure[15] and ionic motions[16] of solid ionic conductors. As an element-selective method, sensitive to local interactions, as dipolar interactions and nuclear electric quadrupolar couplings, NMR studies can provide valuable information on the atomic and molecular motions that modulate these interactions. During the past decades, the ion dynamics of metal halide-doped lithium borate and tellurite glasses have been characterized by detailed temperature-dependent line shape and spin−lattice relaxation rate measurements.[17–23] In general, the cations are found to be mobile, whereas the extent of anion mobility is often uncertain. In contrast to the detailed dynamical characterization, there is presently little information on the local structure of these materials. Specifically the structural role of the lithium halide

in alkali borate glasses has remained unclear. In many fast-ionic glasses, the alkali or silver halide added to an oxide glass simply serves as a dopant, merely functioning as a source of mobile ions.[24–29] As for alkali fluoride in borate glasses, the structural role of the halide ions remains controversial. While ¹¹B wide-line NMR studies suggest no structural modification of the borate network by addition of LiF and LiCl in lithium halide borate glasses,[18] the opposite conclusion has been reached by other researchers, based on NMR[30] and XPS studies[12] on related systems. High-resolution solid-state NMR presents an ideally suited technique for addressing this issue. Both chemical shifts, measured by magic-angle spinning (MAS) and magnetic dipole−dipole interactions, measured by double-resonance techniques, such as spin echo double resonance (SEDOR),[31] and rotational echo double resonance (REDOR),[32] are highly sensitive to the local environments. REDOR reintroduces the heteronuclear magnetic dipole−dipole coupling between two nuclear species X and Y, which is normally averaged out by MAS, by the effect of coherent 180° pulse trains applied to these nuclei during the rotor period. The experiment is conducted in two steps.[32] In the first step, the signal of the observe nucleus X is detected by a rotor synchronized Hahn spin echo sequence, producing a signal with intensity S_0. In the second step, the X−Y dipolar interaction is recoupled by applying π pulse trains to the Y spins during the dipolar recoupling time $N \times T_r$ (the product of the number of rotor cycles and the rotor period). As a result of this recoupling, the signal of the observed nuclei is decreased to an intensity S. A plot of the normalized difference signal $\Delta S = (S_0 - S)/S_0$ against $N \times T_r$ constitutes a "REDOR curve", from which the dipolar coupling strength can be quantified. During the past 10 years a number of applications to glasses have been published.[33–36] In the present paper we use this strategy as one of several complementary techniques within the first multinuclear high-resolution NMR study of the

* To whom correspondence should be addressed.
† Westfälische Wilhelms−Universität Münster.
‡ Università degli Studi di Milano-Bicocca.
§ Universidade de São Paulo.

The Ion-Conducting Glass System B_2O_3−PbO−LiF

J. Phys. Chem. C, Vol. 112, No. 28, 2008 **10463**

B_2O_3−PbO−LiF glass system. On the basis of ^7Li, ^{11}B, ^{19}F, and ^{207}Pb single- and double-resonance experiments on a glass with composition $50B_2O_3$−$10PbO$−$40LiF$, we develop a quantitative structural description of this material. The results outline a general strategy for the structural elucidation of fluoride-containing glasses.

Experimental Section

Sample Preparation and Characterization. Glassy samples of $(50 - x)PbO$−$xLiF$−$50B_2O_3$ with x ranging from 0 to 40 were prepared by conventional mixing and melting oxide and fluoride compounds from high-purity reagent-grade PbO, LiF, and B_2O_3 powders in 10 g batches. All glasses were melted in a platinum crucible in an electrically heated furnace operating at 900 °C. The glasses were cast as rectangular bars in a brass mold. Differential scanning calorimetry (DSC) was used to determine the glass transition temperature, T_g, using a DSC 2090 (TA Instruments) thermal analysis system operated at a heating rate of 10 K/min. The bars were subsequently annealed near T_g for 3 h and allowed to cool to room temperature in the furnace. The composition of each sample was determined by Induced Coupled Plasma (ICP) analysis (see Table 2). All the glasses were characterized by X-ray powder diffraction and were found to be amorphous.

The electrical conductivity was measured by using the impedance spectroscopy technique. The glasses were cut in rectangular samples and the electric contact was made with use of a silver paint. The impedance measurements were performed in the frequency range from 1 Hz to 10 MHz, with an applied potential of 0.75 V, using a Solartron 1260 Impedance Analyzer. These ac measurements were taken isothermally, from room temperature up to 600 K. Resistance values corresponding to the direct-current (dc) regime were obtained by fitting the impedance spectra and subsequently converted into electrical conductivity considering sample dimensions.

Ion Dynamics Characterization by Solid-State NMR. The lithium and fluoride ion dynamics were probed by variable-temperature line shape studies. The ^7Li NMR measurements were conducted on a Varian-400 MHz INOVA spectrometer operating at 155.4 MHz, using a wide line Varian probe at a temperature range of 140−353 K. The static ^7Li line shape was obtained from the Fourier transform of the decaying part of a Hahn spin echo, using CYCLOPS phase cycling. A relaxation delay of 60 s and a $\pi/2$ pulse length of 4 μs were used. The ^{19}F NMR line shapes were measured in the temperature range of 290−700 K, using a pulsed NMR spectrometer operating at 36 MHz and equipped with a TECMAG NMR-kit. For the NMR measurements the samples were placed inside vacuum sealed 6 mm diameter quartz tubes. A variable-temperature probe equipped with a platinum coil and an electric furnace was used for the high-temperature ^{19}F NMR measurements. To standardize the NMR measurements the data were collected beginning at the lowest temperature and increasing the temperature to above the glass transition temperature of the glass sample (T_g = 352 °C). For each high-temperature run, a fresh sample was used. The ^{19}F NMR spectra were obtained by Fourier transformation of the averaged free induction decay signal. The length of the $\pi/2$ pulse was optimized at each temperature and was in the range from 1.9 to 2.7 μs.

Structural Characterization by Solid-State NMR. Solid-state NMR spectra were obtained on a Bruker DSX 400, a Bruker DSX 500, and a Varian Unity INOVA 400 spectrometer. All measurements were conducted at room temperature unless stated otherwise. ^{11}B MAS NMR spectra were acquired at 160.4

MHz in a 4 mm MAS NMR probe operated at a spinning speed of 15 kHz. Single pulses of 0.6 μs length (30° solid flip angle) and a recycle delay of 15 s were used. Triple-Quantum MAS NMR[37] spectra were acquired by using the three-pulse (ZQ-filtering) sequence,[38] using similar conditions as reported previously.[39] Strong preparation and mixing pulses of 3.5 and 1.25 μs lengths were used, and the soft detection pulse had a 10 μs length. 2D-acquisition was carried out in 400 steps (288 scans, recycle delay 0.5 s), using a t_1 increment of 3.3 ms. Chemical shifts are reported relative to BF_3−Et_2O solution. $^{11}B\{^{19}F\}$ rotational echo double-resonance (REDOR) measurements were conducted at an ^{11}B observation frequency of 128.3 MHz and a ^{19}F recoupling frequency of 376.3 MHz in a 4 mm double-resonance MAS NMR probe operated at a spinning frequency of 15 kHz. The compensated REDOR sequence[40] was used, with π pulse lengths of 6 and 7.4 μs, for ^{11}B and ^{19}F, respectively, and a relaxation delay of 5 s. In this method, the intensity S' is measured when canceling the REDOR effect with an additional π pulse placed on the decoupler channel in the middle of the rotor period. While $S' = S_0$ if the recoupling pulses are perfect, pulse imperfections lead to nonzero difference signals $S_0 - S'$, which can account quantitatively for an underestimation of the REDOR effect under such imperfect conditions.

^7Li MAS NMR spectra were acquired at 194.3 MHz, in a 4 mm MAS probe operated at a spinning frequency of 15 kHz, using 30° pulses of 1 μs length and a recycle delay of 5 s. Chemical shifts are reported relative to a 1 M solution of lithium chloride. Measurements were also conducted at 200 K (recycle delay 30 s). $^7Li\{^{19}F\}$ REDOR curves were measured in a 4 mm MAS probe, operated at a 15 kHz spinning speed in a 9.4 T magnet (observation ^7Li frequency 155.4 MHz and ^{19}F recoupling frequency 376.3 MHz), using the compensated REDOR pulse sequence. The 180° pulse lengths were 4.25 and 3.4 μs on ^7Li and ^{19}F, respectively and a recycle delay of 10 s was used. $^7Li\{^{19}F\}$ SEDOR data were acquired on the same spectrometer, using a 4 mm MAS probe under static conditions, with 180° pulse lengths of 3.8 and 7.8 μs for ^7Li, and ^{19}F, respectively.

Static ^{207}Pb NMR experiments were carried out with the Hahn spin−echo sequence ($\pi/2$−τ−π−τ−acquire) with $\pi/2$ pulse length of 4 μs, spacing $\tau = 30$ μs, and recycle delay of 1 s. This delay was found to result in quantitative signal recovery. Due to the high chemical shift anisotropy of ^{207}Pb in these samples, the spectrum was measured with the variable offset cumulative spectroscopy (VOCS) technique,[41,42] previously applied to ^{207}Pb NMR studies of glasses and ceramics.[43,44] Each spectrum was obtained by coadding the Fourier transforms of signals measured with different irradiation frequencies, separated by 60 kHz. Typically, eight irradiations were enough to cover the whole spectral range, taking 70000 transients for each echo signal. The isotropic shift of solid lead nitrate was used as chemical shift reference (-3491.6 ppm with respect to tetramethyllead). $^{207}Pb\{^{19}F\}$ spin echo double-resonance (SEDOR) data were measured at resonance frequencies of 83.7 and 376.6 MHz, respectively, using 180° pulse lengths of 10 and 7.8 μs for the ^{207}Pb and the ^{19}F resonance, respectively, a dipolar evolution time of 100 μs, and a relaxation delay of 1 s (70000 scans). ^{19}F MAS NMR spectra were obtained on the Bruker DSX-400 spectrometer interfaced with a 4.7 T magnet (observation frequency 188.2 MHz), in a 2.5 mm probe operated at a spinning frequency of 25 kHz, using a rotor-synchronized Hahn spin echo sequence. The 180° pulse length was 5.8 μs, and a relaxation delay of 10 s was used. Spectra were acquired at
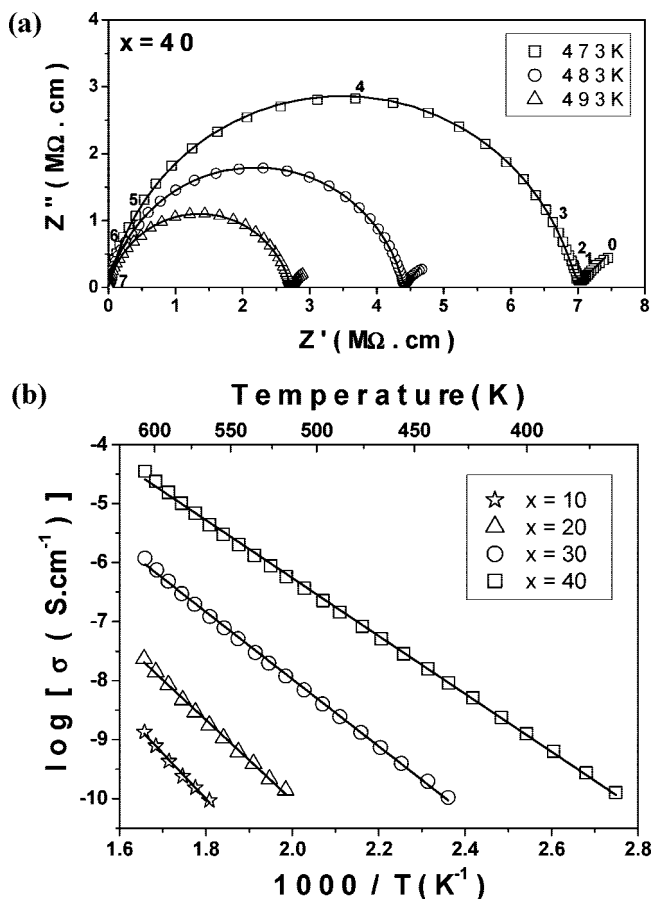
(a)

(b)

Figure 1. (a) Impedance diagrams of $50B_2O_3-10PbO-40LiF$ for T = 473, 483, and 493 K. The solid lines are the theoretical curves obtained by fitting and the numbers indicate the logarithm of signal frequency. (b) Temperature dependence of the electrical conductivity of $50B_2O_3-(50 - x)PbO-xLiF$ glass (x = 10, 20, 30, and 40). The electrical conductivities were determined from the arc in the impedance diagram.

variable evolution times, corresponding to different multiples of the rotor period. Chemical shifts are reported relative to $CFCl_3$, using solid AlF_3 as a secondary standard.

For quantifying the fluorine content in the sample, a mixture consisting of equal masses of Fluoroapatite ($Ca_5(PO_4)_3F$, FAP) and the glass was prepared by carefully grinding 32.8 mg of FAP with 32.8 mg of glass. It was confirmed by thermogravimetry (temperature range 25−300 °C) that neither material contained any significant amount of surface adsorbed water. ^{19}F MAS NMR spectra of 20.8 mg of this mixture were recorded with both single-pulse as well as rotor-synchronized spin echo acquisition. The center of irradiation was set at −172 ppm vs $CFCl_3$. [19]F rotor-synchronized Hahn spin echo experiments were

conducted with use of a 180° pulse length of 4.9 μs and a relaxation delay of 40 s. This relaxation delay was found to yield quantitatively representative results. To assess the possible influence of differential spin−spin relaxation, two separate experiments were done, with the 180° pulse positioned after one and two rotor periods (evolution times of 80 and 160 μs, respectively). The spectra were fitted to Gauss/Lorentz curves, using the DMFIT simulation routine.[45] For each spectral component, one set of spinning sidebands was included in the analysis.

[19]F{[11]B} REDOR data were acquired at 470.4 MHz, in a 2.5 mm probe operated at a spinning frequency of 25 kHz, using 180° pulses of 5.2 and 3.0 μs for ^{19}F and [11]B nuclei, respectively, and a relaxation delay of 40 s. [19]F{[7]Li} REDOR data were obtained under closely similar conditions (180° pulse lengths of 5.5 and 3.4 μs for ^{19}F and [7]Li, respectively).

Results: Data Analysis and Interpretation

Electrical Conductivity Measurements. Impedance spectra of $50B_2O_3-10PbO-40LiF$ glass are presented in Figure 1a. Just one semicircle is resolved and it is possible to observe that the electrode polarization causes a slight contribution at frequencies lower than 100 Hz. Similar spectra were observed for the other compositions. The arcs are depressed, indicating a deviation from the Debye behavior, which is expected for glassy samples. A simple model was employed to represent the electrical response. In the equivalent circuit proposed the arc from the experimental data was represented by a parallel combination of a resistance (R_{Glass}) and a constant-phase element (CPE_{Glass}) and the electrode represented by a CPE.[46–48] The R_{Glass} values were obtained from each fitting at a specific temperature and subsequently normalized by using a geometrical factor (area/thickness). The theoretical curves, plotted in Figure 1a (solid lines), are in excellent agreement with the experimental responses, thus indicating the adequacy of the proposed model.

Figure 1b shows the dependence of the electric conductivity on reciprocal temperature, measured from 350 to 600 K for different glass compositions. The data follow the Arrhenius law,

$$\sigma(T) = \sigma_0 \exp(-E_a/k_B T)$$

where σ_0 is a pre-exponential factor and E_a, k_B, and T represent the apparent activation energy for the conduction process, Boltzmann's constant, and temperature, respectively. Table 2 summarizes the electrical conductivities measured at 603 K and the activation energies.

Variable-Temperature Static Line Shape Analysis. Table 2 summarizes the results of the macroscopic characterization of these glasses. Among this group, clearly the sample with the maximum LiF content has by far the largest electrical conductivity, yielding an activation energy of 0.97 eV (see

TABLE 1: Chemical Analysis Results of Pb, B, and Li Contents for the Glassy Samples Compared to the Nominal Values in Weight Percent Measured for $(50 - x)PbO-xLiF-50B_2O_3$ Glasses

| sample composition | weight (%) | | | | | |
| | **Pb** | | Li | | **B** | |
x	nominal	exptl	nominal	exptl	nominal	exptl
10	65.4	66.6	0.5	0.4	8.5	8.3
15	62.1	65.1	0.9	0.7	9.2	8.5
20	58.1	59.8	1.3	1.1	10.1	9.8
25	53.4	55.1	1.8	1.6	11.1	10.8
30	47.5	51.5	2.4	2.2	12.4	11.3
35	40.2	42.1	3.1	3.1	13.9	13.4
40	30.7	32.8	4.3	4.1	16.0	15.1

The Ion-Conducting Glass System B$_2$O$_3$−PbO−LiF

J. Phys. Chem. C, Vol. 112, No. 28, 2008 **10465**

(a)

(b) **(c)**
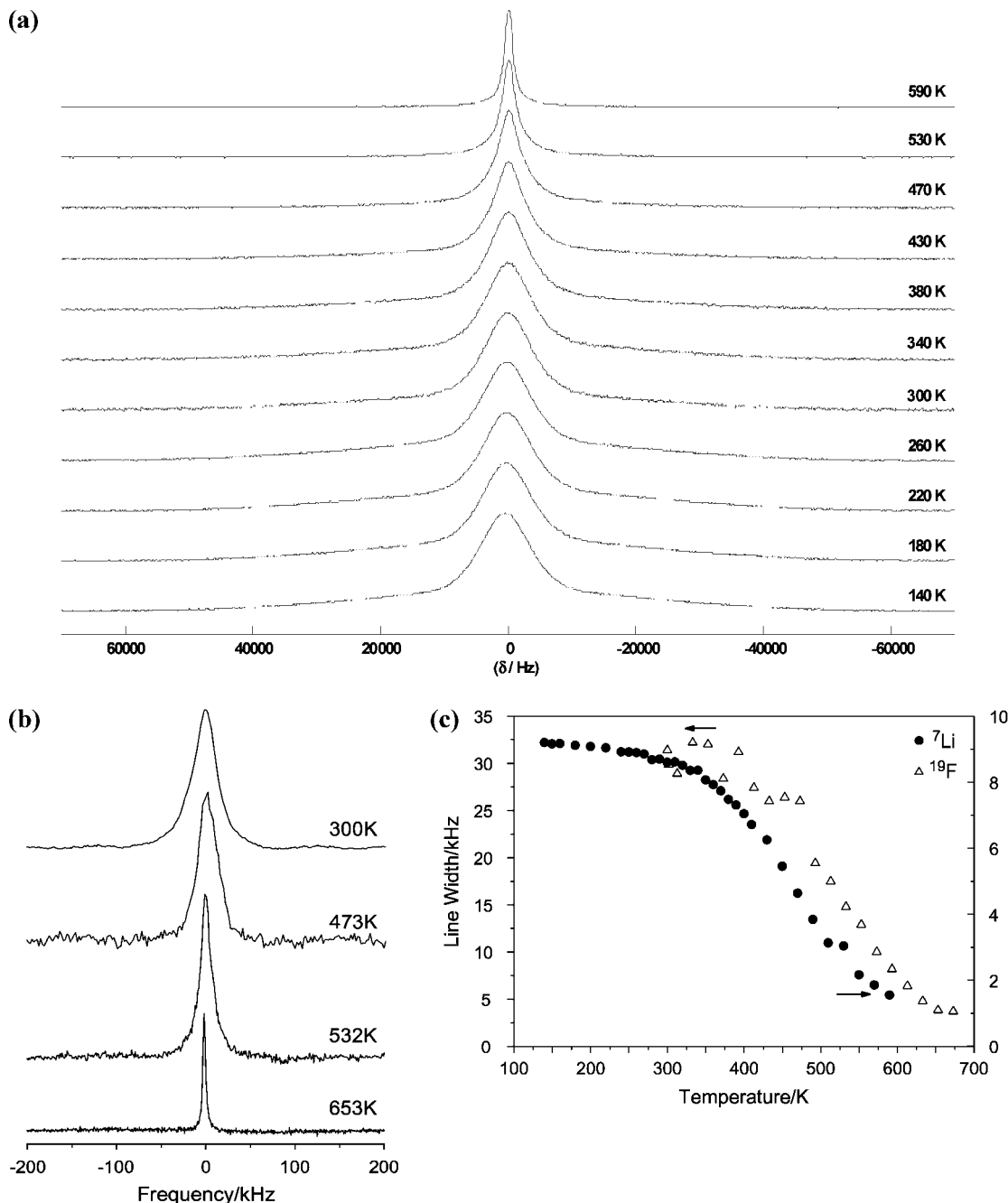
Figure 2. (a) Temperature dependence of the static ^{7}Li NMR line shapes in 50B$_2$O$_3$−10PbO−40LiF glass. (b) Temperature dependence of the ^{19}F static NMR spectral line shapes in 50B$_2$O$_3$−10PbO−40LiF glass. (c) Temperature dependences of the static ^{7}Li and ^{19}F NMR line widths in 50B$_2$O$_3$−10PbO−40LiF glass.

Figure 1b). The individual cation and anion contributions to the electrical conductivity can be assessed by element-selective ion mobility studies, featured by variable-temperature ^{19}F and ^{7}Li NMR line shape analyses (see Figure 2, panels a and b). Figure 2c shows a plot of ^{7}Li and ^{19}F full widths at half-maximum for the 50B$_2$O$_3$−10PbO−40LiF glass. At low temperature the static ^{7}Li NMR line shape, which corresponds to the central $|^1/_2\rangle \leftrightarrow |-^1/_2\rangle$ transition of this quadrupolar nucleus, is dominated by magnetic ^{7}Li−^{7}Li, ^{7}Li−^{19}F, and ^{7}Li−^{11}B dipole−dipole interactions. Above ∼250 K, the lithium mobility increases sufficiently to reduce the magnetic dipole−dipole couplings on the NMR time scale, thus producing a line narrowing. As is typical for glassy materials, the temperature range over which the line width decrease is observed is rather wide, indicating substantial dynamic heterogeneity.[16] A similarly

wide temperature range of line narrowing is observed for the ^{19}F NMR signal. However, Figure 2c indicates that the onset of this line narrowing is shifted to significantly higher temperatures (around 400 K). In view of the ^{7}Li NMR results, the ^{19}F line narrowing effect in this temperature range might be attributable to the cancelation of the ^{7}Li dipolar fields probed by the ^{19}F nuclei due to lithium ion motion. On the other hand, the narrow line observed above 650 K clearly indicates isotropic fluoride ion mobility at this temperature. From Figure 2c we can conclude that the cationic motion is more easily activated than that of the fluoride ions. As discussed below in more detail, the lower fluoride ion mobility may be related to the interaction (binding) of fluoride with the glass network former species.

High-Resolution ^{11}B NMR. In the ^{11}B MAS NMR spectrum (Figure 3a) the contributions of four- and three-coordinated
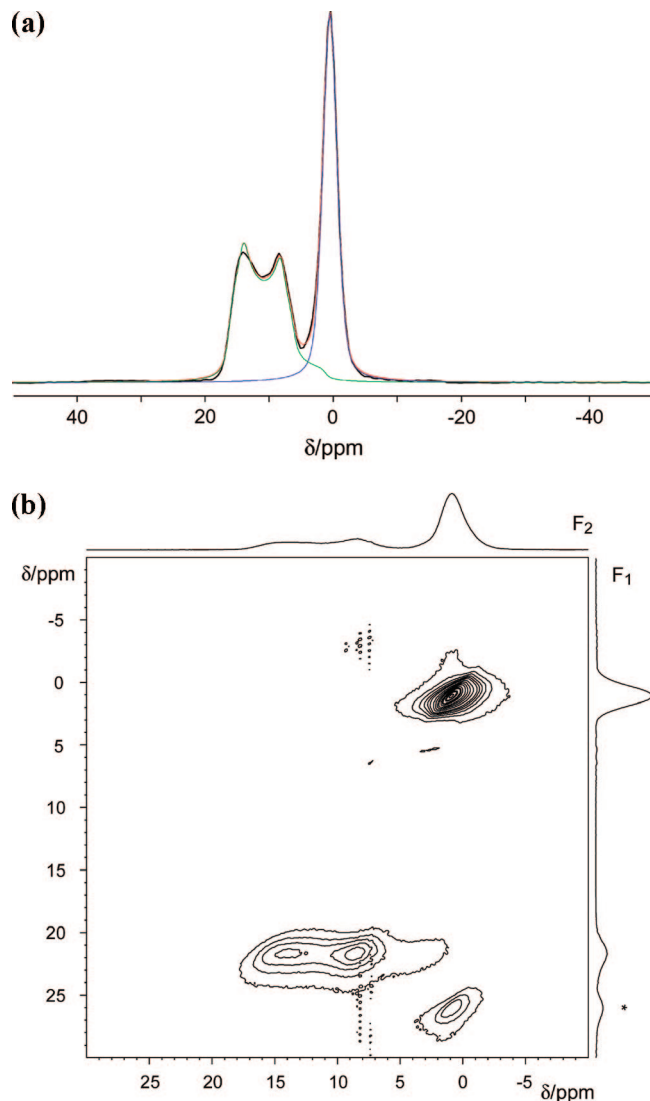
(a)

(b)

Figure 3. (a) ^{11}B MAS NMR spectrum of $50B_2O_3-10PbO-40LiF$ glass. Solid green and blue curves are line shape deconvolution components, and their sum is displayed as the red curve. (b) ^{11}B TQ-MAS NMR spectrum of $50B_2O_3-10PbO-40LiF$ glass. A spinning sideband is marked by an asterisk.

boron units are readily resolved. While the four-coordinated boron units produce a sharp resonance at 1.0 ppm, the line shape attributed to the 3-fold boron sites is broadened by second-order nuclear electric quadrupolar effects, created by a significant electric field gradient at the boron nuclei. Figure 3a also includes a simulated spectrum, based on the parameters nuclear electric quadrupole coupling constant $C_Q = 2.59$ MHz, electric field gradient asymmetry parameter $\eta = 0.25$, and isotropic chemical shift $\delta_{iso} = 17.6$ ppm. The fraction N_4 of the four-coordinate boron species, as determined by peak area analysis, amounts to 0.49 ± 0.03. This value is significantly higher than that expected from the ratio $R = \text{mol \% PbO/mol \% } B_2O_3 = 0.2$ in the present sample, assuming that LiF simply functioned as a dopant species. This discrepancy can be explained by the assumption that LiF actively participates in the network modification process, according to the reactions:

$$BO_{3/2} + LiF \rightarrow BO_{3/2}F^-Li^+ \quad (1a)$$

$$2BO_{3/2} + LiF \rightarrow BO_{2/2}F + BO_{4/2}{}^-Li^+ \quad (1b)$$

Enhanced N_4 values observed in NMR data on $NaF-B_2O_3$ glasses have been explained in a similar vein;[30] however, the

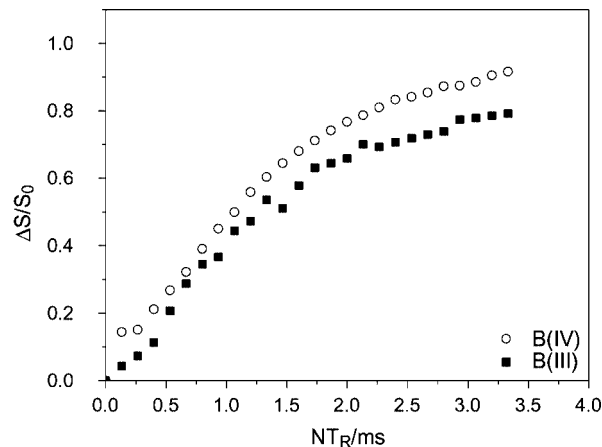**Figure 4.** $^{11}B\{^{19}F\}$ REDOR curves obtained on $50B_2O_3-10PbO-40LiF$ glass.

TABLE 2: Glass Transition and Crystallization Temperatures, T_g and T_x, respectively, Electrical Conductivities, σ, Measured at 603 K, and Corresponding Activation Energies, E_a, Measured for $50B_2O_3-(50 - x)PbO-xLiF$ Glasses

x	T_g [K]	T_x [K]	σ [S·cm^{-1}]	E_a [eV]
0	667	798	4.2×10^{-10}	1.55
10	650	795	1.3×10^{-9}	1.53
20	645	788	2.3×10^{-8}	1.35
30	629	720	1.2×10^{-6}	1.13
40	625	733	3.6×10^{-5}	0.97

possibility of fluoride loss during melting and its corresponding replacement by oxide ions opens up another possible explanation for such enhanced N_4 values; this issue will be addressed later on the basis of a detailed fluoride quantification experiment.

Because the nominal F/B ratio in the present sample is 0.4, only a fraction of the boron atoms can be F-bonded. Thus, both $BO_{4/2}{}^-$ and $BO_{3/2}F^-$ species are expected, for which distinct resonances might be expected in ^{11}B MAS NMR; in addition, the formation of $BO_{2/2}F$ units is possible. In an attempt to resolve these different species, a 2D-TQMAS ^{11}B NMR experiment was carried out (Figure 3b). While this spectrum indeed presents a significantly enhanced resolution in comparison to the regular MAS NMR spectrum, no distinguishable types of three- and four-coordinate boron environments can be resolved. Analysis of the TQMAS spectrum yields the isotropic chemical shift δ_{iso} and the second-order quadrupolar effect $SOQE = C_Q(1 + \eta^2/3)^{1/2}$. The four-coordinated boron sites are characterized by $\delta_{iso} = 0.9 \pm 0.1$ ppm and $SOQE = 470 \pm 20$ kHz. The tilt observed for the cross-peak in the 2D spectrum reveals a distribution of isotropic chemical shifts, indicative of a distribution of local environments (and possibly the contribution of BO_3F^- units). For the three-coordinated boron sites, the analysis yields $\delta_{iso} = 17.7 \pm 0.5$ ppm and $SOQE = 2.63 \pm 0.04$ MHz, respectively, in good agreement with the results from single-pulse MAS NMR.

To explore the question of boron–fluorine bonding further, $^{11}B\{^{19}F\}$ REDOR experiments were carried out. While the data, shown in Figure 4, do not allow a clear distinction between F-bonded and non-F-bonded boron species on the basis of chemical shifts, they do reveal, at least on a qualitative basis, that both types of boron sites experience strong ^{19}F dipolar fields, consistent with the proposed network modifier role of LiF. Attempts at distinguishing the static line shapes of the F-bonded B atoms from those of the non-F bonded B atoms on the basis
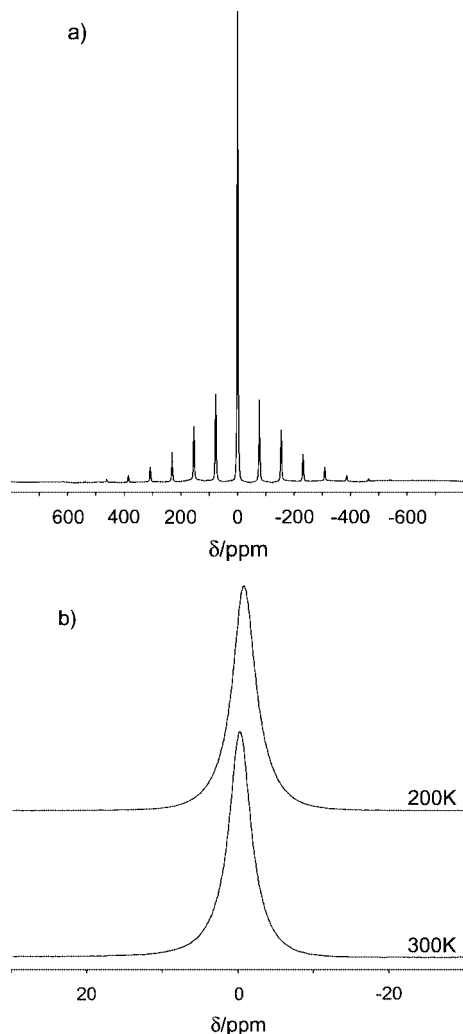
Figure 5. ^7Li MAS NMR spectra of $50B_2O_3-10PbO-40LiF$ glass: (a) full line shape at 300 K, revealing both the MAS central band and the spinning sideband manifold; (b) MAS central band at 200 and 300 K.

of $^{11}B\{^{19}F\}$ SEDOR difference experiments were also unsuccessful (data not shown), as it was not possible to resolve these dipolarly broadened signals from those of the trigonally coordinated boron species, which are broadened by second-order quadrupolar effects.

^7Li MAS and $^7Li\{^{19}F\}$ REDOR. Figure 5 shows the ^7Li MAS NMR spectrum of the sample. A single sharp line at -0.3 ± 0.1 ppm suggests the formation of a single lithium environment. The sharp central resonance, which corresponds to the $|^1/_2\rangle \leftrightarrow |-^1/_2\rangle$ Zeeman transition, is flanked by a set of spinning sidebands, which arise from the influence of MAS on the other $|\pm^1/_2\rangle \leftrightarrow |\pm^3/_2\rangle$ "satellite transitions", which are anisotropically broadened by the nuclear electric quadrupolar interactions in the limit of first-order perturbation theory. The nuclear electric quadrupolar coupling constant, as estimated from the overall frequency range of the satellite peaks, is 200 ± 20 kHz. To exclude the possibility that the single sharp line arises from rapid chemical exchange effects due to lithium ionic motion, a MAS NMR spectrum was obtained at 200 K. Even at this temperature only a single peak is observable (at -0.9 ± 0.1 ppm). While the lithium ions probably have various different coordination environments with different O/F proportions in this glass sample, the chemical shift differences between those are probably too small to be resolved by MAS NMR. The extent of lithium/fluorine interaction can be evaluated on the basis of $^7Li\{^{19}F\}$
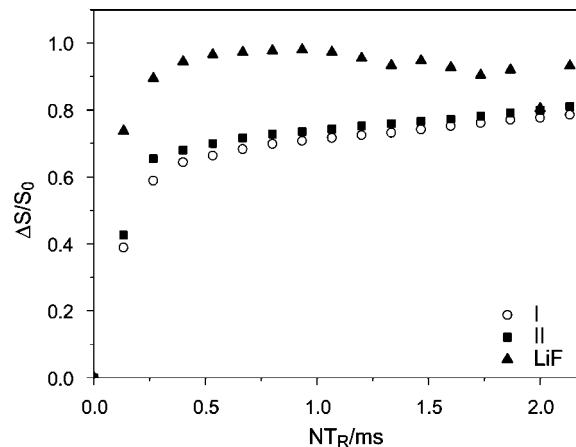

Figure 6. $^7Li\{^{19}F\}$ REDOR curves of $50B_2O_3-10PbO-40LiF$ glass (two separate data sets, I and II) and crystalline LiF.

rotational echo double-resonance (REDOR) studies. Figure 6 compares the REDOR curves obtained on the glass (two separate data sets) with one measured for a crystalline LiF sample. In principle, the strength of the magnetic dipole–dipole coupling can be quantitatively characterized by applying a curvature analysis at short recoupling times.[33–36,40] In the present study, such an analysis is not possible, however, because of the steep rise of the curve owing to the extremely strong dipole–dipole coupling, limiting the analysis to a discussion of qualitative features only. In this vein, Figure 6 clearly indicates, first of all, that the $^{19}F-^7Li$ dipole–dipole coupling, albeit very strong, is still significantly weaker than in the model compound LiF. Second, the data obtained for the glass suggest a two-component behavior: the rapid initial increase of the REDOR difference signal can be attributed to lithium ions having fluoride in their first coordination sphere. In contrast, the long-time behavior must be attributed to lithium ions that are only weakly interacting with fluoride. We assign those lithium ions contributing to the long-time decay to species having exclusively oxygen in their coordination spheres. From the shape of the REDOR curve we estimate that about $30(\pm5)\%$ of the lithium ions present are not F-bonded.

$^7Li\{^{19}F\}$ SEDOR. The average $^7Li-^{19}F$ dipole–dipole interaction strength can be estimated more accurately on the basis of spin echo double-resonance (SEDOR) experiments, the results of which are shown in Figure 7. In this experiment, which can be considered the static version of REDOR, the dephasing rate of the ^7Li Hahn spin echoes, $F(2t_1)/F(0)$, is compared with the dephasing rate $I(2t_1)/I(0)$ of these echoes in the presence of a ^{19}F-180° pulse, transmitted at the same time as the 180° refocusing pulse is applied to the ^7Li nuclei. The ^{19}F-180° pulse recouples the $^7Li/^{19}F$ dipole–dipole interaction, leading to an accelerated ^7Li Hahn spin echo decay. For a multispin system, the interaction can be modeled to yield a Gaussian decay according to:[49]

$$\frac{I(2t_1)}{I(0)} = \frac{F(2t_1)}{F(0)} \exp[-0.5M_2(2t_1)^2] \qquad (2)$$

In this expression, the $F(2t_1)/F(0)$ ratio is the normalized spin echo decay in the absence of the ^{19}F inversion pulse; this curve is well-fitted by an exponential function. Panels a and b of Figure 7 show the experimental data, both for the glass and for the crystalline model compound LiF. For the latter, an analysis of the experimental data according to eq 2 yields $M_2(^7Li-^{19}F) = 3400 \times 10^6$ rad^2/s^2. The rather poor agreement with the theoretically calculated value from the crystal structure, using

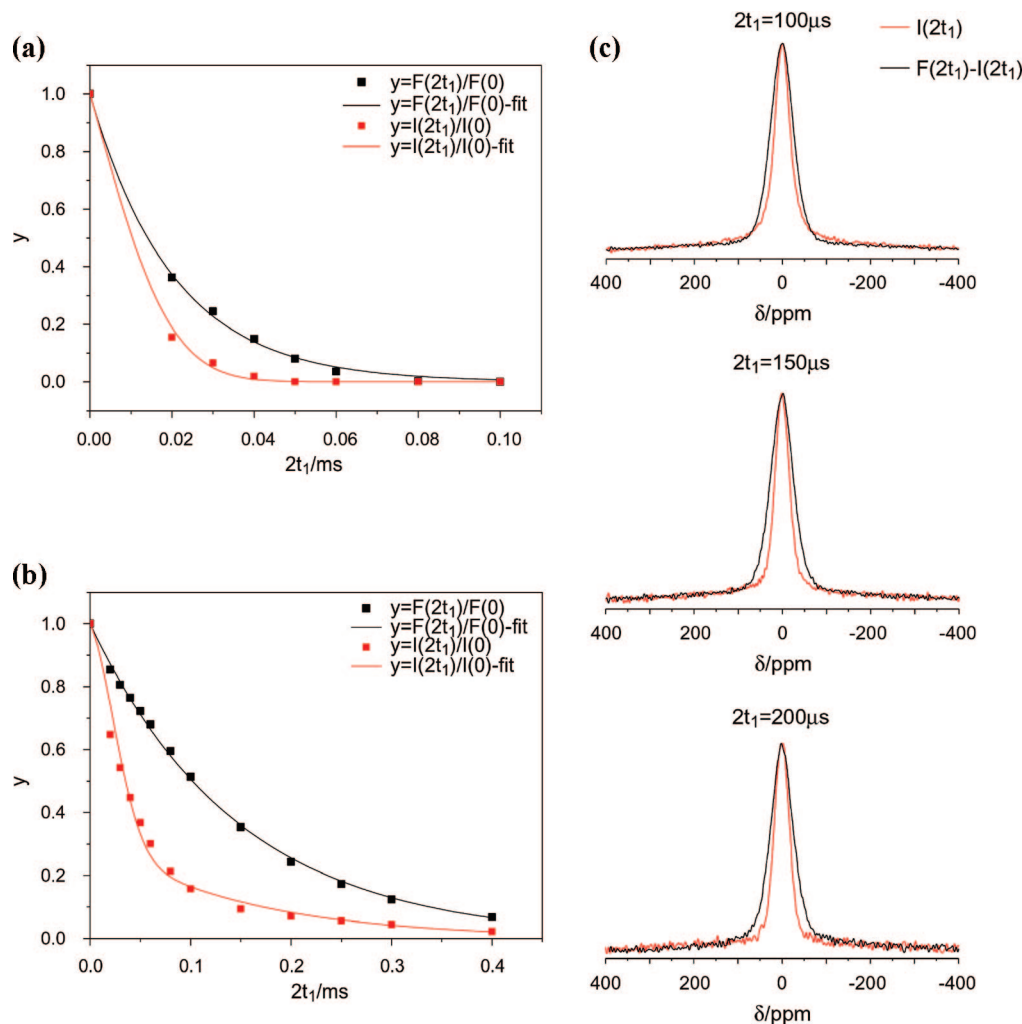**Figure 7.** (a) $^7\text{Li}\{^{19}\text{F}\}$ SEDOR results on crystalline LiF. (b) $^7\text{Li}\{^{19}\text{F}\}$ SEDOR results on $50\text{B}_2\text{O}_3-10\text{PbO}-40\text{LiF}$ glass. (c) Spectral comparisons of the Fourier Transforms of $I(2t_1)$ (red) and $F(2t_1) - I(2t_1)$ (black) for three different dipolar evolution times $2t_1$. The differences in the corresponding line widths are evident.

the van Vleck equation[50] ($M_2 \approx 1500 \times 10^6$ rad^2/s^2), can be explained on the basis of the extremely strong dipole−dipole coupling, limiting the analysis to very few data points, where the majority of the dephasing has already taken place. The Gaussian approximation implicit in the analysis according to eq 2 may be inappropriate here. For the glass, the situation looks more favorable; however, the data (like the REDOR results) indicate that the analysis according to eq 2 is not applicable here either, because of the bimodal character of the $^7\text{Li}-^{19}\text{F}$ dipolar coupling. Rather, we must take into account that a sizable fraction C of the lithium ions has no ^{19}F in their first coordination sphere. On the time scale of the SEDOR experiment conducted in the present study, these lithium ions do not contribute to the SEDOR decay. Thus, we replace expression 2 with the equation

$$\frac{I(2t_1)}{I(0)} = \frac{F(2t_1)}{F(0)}\{C + (1 - C)\exp[-0.5M_2(2t_1)^2]\} \quad (3)$$

where C and M_2 are adjustable parameters. Least-squares fitting yields the result $C = 0.32 \pm 0.03$ and $M_2 = (1240 \pm 140) \times 10^6$ rad^2/s^2, the latter obtained from the initial decay (the first four data points). The value of C is in excellent quantitative agreement with the REDOR result, which also suggests that about 30% of the lithium ions do not have fluoride ions in their first coordination sphere. While the M_2-value is in proximity of the theoretically expected value for lithium fluoride, a closer

inspection of the ratio $I(2t_1)/F(2t_1)$ as a function of the $2t_1$ data range shows a systematic decrease of M_2 with increasing data range. This result suggests that there is a distribution of $^7\text{Li}-^{19}\text{F}$ dipole−dipole couplings. This finding is not unexpected as the numbers of fluorine and oxygen ligands in the first coordination sphere of the lithium ions are most likely subject to variation. Figure 7c illustrates that at intermediate dipolar evolution times ($100~\mu s \leq 2t_1 \leq 200~\mu s$) the spectral line shapes $I(2t_1)$ and $F(2t_1) - I(2t_1)$ are quite distinct. Within this range of evolution times, the F-bonded Li species have completely decayed in the SEDOR signal $I(2t_1)$, while their contribution is emphasized in the $F(2t_1) - I(2t_1)$ difference signal. As Figure 7c illustrates, the latter is significantly broader than the former, reflecting the effect of the heteronuclear $^{19}\text{F}-^7\text{Li}$ magnetic dipole−dipole interactions.

Both Figures 6 and 7 reveal that in the present glass system the dipolar coupling is significantly weaker than in crystalline LiF. This result argues against the formation of larger LiF-like domains in these glasses, and is consistent with the conclusion that lithium fluoride participates actively in the network transformation process.

Static ^{207}Pb and $^{207}\text{Pb}\{^{19}\text{F}\}$ SEDOR. Figure 8a summarizes the static ^{207}Pb NMR spectra of three samples with compositions $(\text{B}_2\text{O}_3)_{50}-(\text{PbO})_{50-x}-(\text{LiF})_x$, indicating significant chemical shift changes as a function of composition. One possible explanation
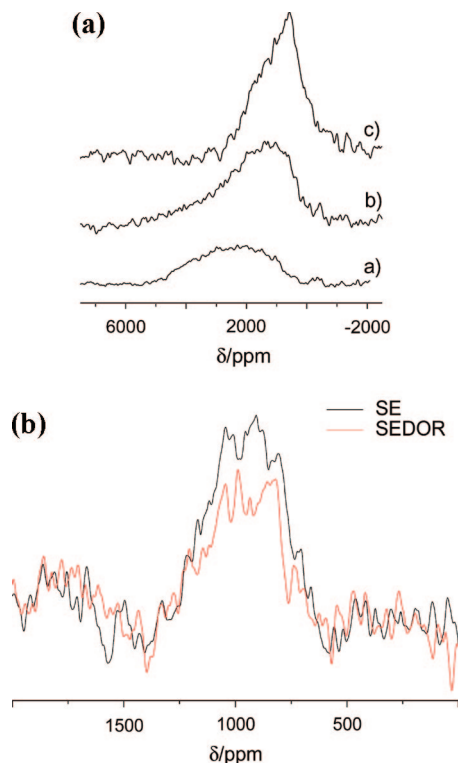
The Ion-Conducting Glass System B$_2$O$_3$−PbO−LiF

J. Phys. Chem. C, Vol. 112, No. 28, 2008 **10469**

Figure 8. (a) Static ^{207}Pb NMR spectra of 50B$_2$O$_3$−(50 − x)PbO−xLiF glasses: (a) x = 0, (b) x = 20, (c) x = 40. (b) ^{207}Pb{^{19}F} SEDOR data, obtained at a dipolar evolution time of 100 μs for 50B$_2$O$_3$−10PbO−40LiF glass. Black curve: ^{207}Pb spin echo Fourier Transform. Red curve: 207Pb spin echo Fourier Transform in the presence of the ^{19}F π-pulse.

Figure 9. ^{19}F rotor-synchronized MAS NMR experiments undertaken on 50B$_2$O$_3$−10PbO−40LiF glass. (a) Stack plot of the Fourier transforms as a function of dipolar evolution time. Spinning sidebands are indicated by asterisks. (b) Plot of normalized intensity as a function of dipolar evolution time. Note the significantly faster decay of the −198 ppm resonance.

invokes the presence of strong Pb−F bonding interactions which increase with increasing x. To explore this possibility, Figure 8b presents the results of a ^{207}Pb{^{19}F} SEDOR experiment, carried out on the x = 40 sample at a dipolar evolution time of 100 μs. Even though only poor signal-to-noise ratio is obtained, and the ^{207}Pb NMR line shape is strongly distorted by the limited excitation window, some useful semiquantitative conclusions are possible from this experiment. The SEDOR signal is visibly reduced, indicating the presence of ^{207}Pb−^{19}F dipole−dipole couplings. Assuming a Gaussian decay of the ^{207}Pb signal in the dipolar field of the ^{19}F nuclei, we estimate a second moment value of $(29 \pm 10) \times 10^6$ rad^2/s^2 from the ratio $I(2t_1)/F(2t_1)$ measured at a dipolar evolution time of 100 μs (the large error reflects the poor signal-to-noise ratio obtained in this experiment. Assuming an internuclear distance of 255 pm (as in crystalline lead fluoride), the second moment contributed by a single Pb−F bond is about 20×10^6 rad^2/s^2. Thus, based on the experimental value, we estimate that, on average, each Pb^{2+} ion has 1.5 ± 0.5 fluoride ions in its first coordination sphere, the remainder being oxygen. On the basis of the glass composition, this value is consistent with a random distribution of F in relation to Pb and argues against a preferential attraction of F by the Pb^{2+} ions (formation of PbF$_2$-like domains). As a matter of fact, strong ^{207}Pb NMR line shape changes have also been seen in binary lead borate glasses, and attributed to a transition of the lead oxide from a network modifier role (at low PbO contents) to a network former role (at high PbO contents).[51] Most likely, the same explanation applies in the present ternary glasses.

^{19}F MAS, ^{19}F{^{7}Li} REDOR, and ^{19}F{^{11}B} REDOR. Figure 9a shows ^{19}F MAS NMR spectra, acquired in the form of rotor-synchronized Hahn spin echoes. Two distinct resonances near
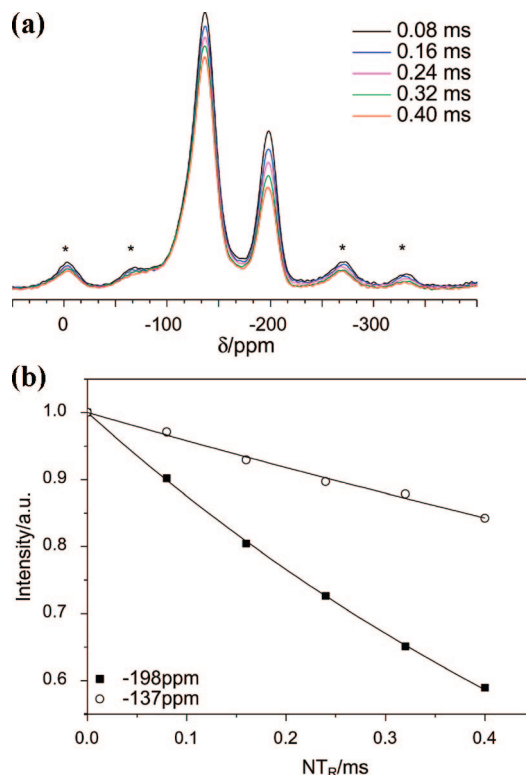
−137 and −198 ppm are detectable. In this experiment the number of rotor cycles prior to signal detection was systematically varied, and the evolution of the signal intensity as a function of waiting time between the 90° preparation pulse and the MAS echo detection is shown in Figure 9b. Clearly, the −198 ppm signal decays significantly more rapidly than the −137 ppm signal. As the signal decay under these conditions is primarily dominated by the strength of the homonuclear ^{19}F−^{19}F dipole−dipole interactions, Figure 9b indicates that the latter are significantly stronger for the F species contributing to the −198 ppm signal than those for the F species contributing to the −137 ppm signal. Figure 10a summarizes results from ^{19}F{^{7}Li} REDOR and ^{19}F{^{11}B} REDOR experiments, obtained with a dipolar evolution time of 80 μs. On the basis of the stronger reduction of the −198 ppm signal in the ^{19}F{^{7}Li} REDOR experiment, we assign this species to a fluoride in a lithium-dominated environment; this assignment is also consistent with the isotropic chemical shift of crystalline LiF (−203 ppm).[52] In the same vein, the signal at −137 ppm is assigned to a boron-bonded fluorine species, based on the strong ^{19}F{^{11}B} REDOR effect. Panels b and c of Figure 10 summarize the complete REDOR curves, indicating that the partial selectivity is observed over the full range of dipolar evolution times. Unfortunately, a more quantitative analysis of these REDOR curves is not possible, because the line shapes of the "dephaser" nuclei ^{7}Li and ^{11}B are both affected by first-order quadrupolar splittings, producing large off-resonance effects, which reduce the inversion efficiency achieved by the 180° pulses used in these REDOR experiments to an unknown extent.

Fluorine Quantification. Figure 11 shows representative data on the fluorine quantification in the x = 40 glass. The resonance of the fluoroapatite (FAP) standard added to the sample is well
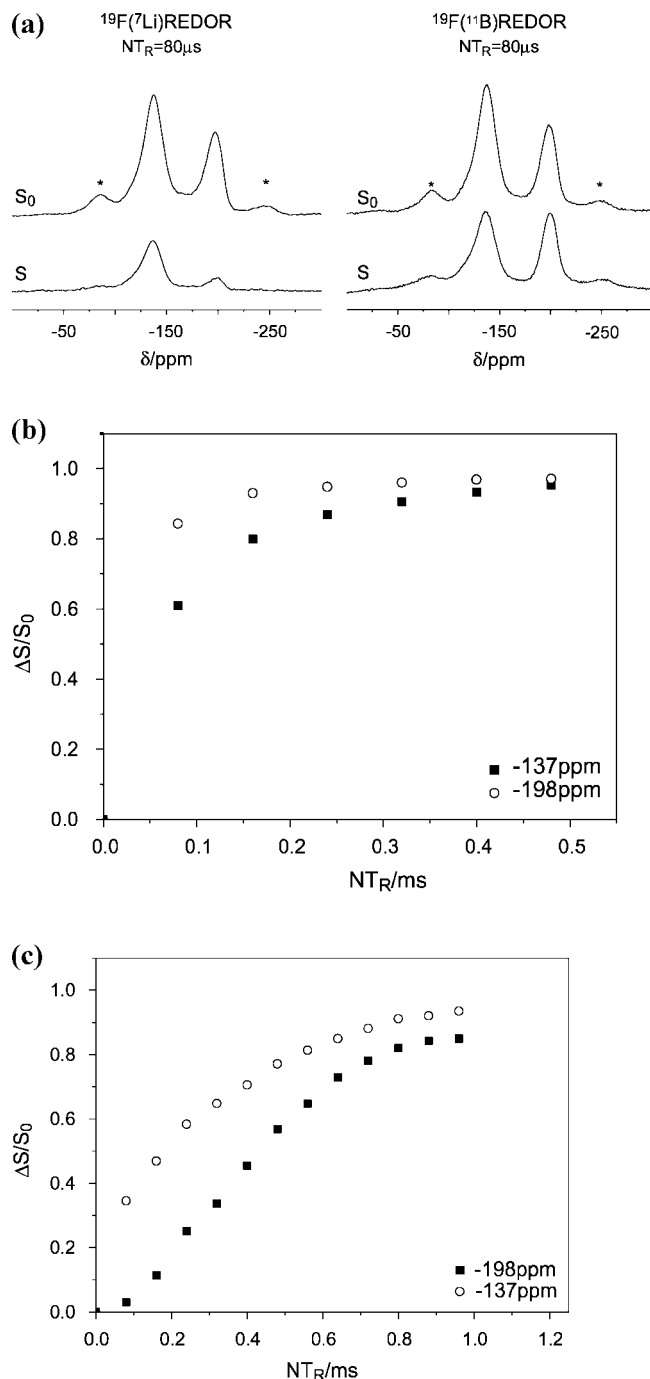
(a)

(b)

(c)

Figure 10. (a) $^{19}F\{^{7}Li\}$ and $^{19}F\{^{11}B\}$ REDOR experiments on $50B_2O_3-10PbO-40LiF$ glass: spectra obtained after a fixed dipolar evolution time of 80 μs. Spinning sidebands are indicated by asterisks. (b) $^{19}F\{^{7}Li\}$ REDOR curves obtained on $50B_2O_3-10PbO-40LiF$ glass. (c) $^{19}F\{^{11}B\}$ REDOR curve obtained on $50B_2O_3-10PbO-40LiF$ glass.

separated at −103 ppm from those of the glass, and at the spinning speed chosen, there is no spinning sideband overlap. The total area attributed to the FAP was found to be 33.7% and 31.9%, in the single pulse and the rotor synchronized echo experiments. In the latter experiments, no significant influence of the evolution time was detected. The results from the rotor synchronized experiments yielded higher quality fits and are considered more reliable (better baseline, absence of phasing errors). On the basis of the fact that FAP contains 3.76 mass % fluorine, the fluorine content of the glass is calculated as 8.04 mass % from the analysis of relative signal areas. The
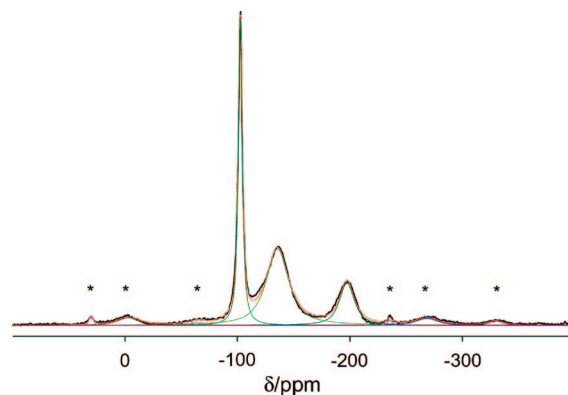

Figure 11. ^{19}F MAS NMR spectrum of a mixture of equal masses of $50B_2O_3-10PbO-40LiF$ glass and fluoroapatite standard. Solid green curves are line shape deconvolution components, and their sum is displayed as the red curve. Spinning sidebands are indicated by asterisks.
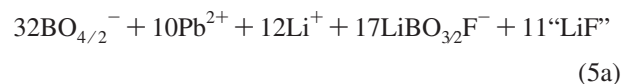
discrepancy to the nominal fluorine content (11.26 mass %) shows that significant fluorine loss has occurred (see Discussion). Losses of such magnitude are not uncommon for fluoride glasses prepared in open atmospheres.
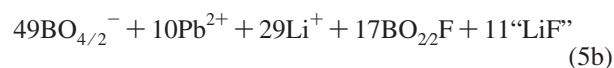
Discussion

A reasonable model of the fluoride loss can be formulated by postulating an exchange reaction of the type

$$B_2O_3 + 6LiF \rightarrow 2BF_3 + 3Li_2O \qquad (4)$$
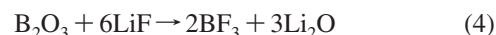
This reaction produces volatile boron trifluoride and lithium oxide, the latter of which can react with additional B_2O_3 network former, leading to the formation of four-coordinated boron species. The extent to which this reaction takes place can be calculated from the experimentally determined fluoride loss, which amounts to 30%. According to this loss, the bulk glass composition $50B_2O_3-10PbO-40LiF$ liberates $4BF_3$, leaving behind an oxyfluoride glass with composition $48B_2O_3-10PbO-28LiF-6Li_2O$. Note that this composition change involves a reduction in relative boron content and an increase in relative Pb content, in general agreement with the chemical analysis results (Table 1). The Li_2O formed in this manner acts as a network modifier species, producing additional four-coordinate boron species. On the basis of these considerations alone, the predicted N_4 value would be 0.33, which is still substantially lower than the experimentally observed value. Thus, fluoride loss alone cannot account for the experimental results. In this connection, the ^{19}F MAS NMR data are significant: roughly 60% of the fluorine species remaining in the glass are present as boron-bonded species, while 40% of the fluorine species occur in the Li-dominated environment contributing to the peak at −198 ppm. Thus the structural model can be refined leading to:

$$48B_2O_3 - 10PbO - 28LiF - 6Li_2O \rightarrow 47BO_{3/2} +$$

$$32BO_{4/2}^- + 10Pb^{2+} + 12Li^+ + 17LiBO_{3/2}F^- + 11\text{"LiF"}$$
$$(5a)$$

or

$$48B_2O_3 - 10PbO - 28LiF - 6Li_2O \rightarrow 30BO_{3/2} +$$

$$49BO_{4/2}^- + 10Pb^{2+} + 29Li^+ + 17BO_{22}F + 11\text{"LiF"}$$
$$(5b)$$

Both reactions 5a and 5b predict $N_4 = 0.50$, in excellent agreement with the experimental value of 0.49. Furthermore,

in both models it is possible that a significant amount of lithium is remote from fluorine, in good agreement with the $^7Li\{^{19}F\}$ REDOR and SEDOR results. As pointed out earlier, independent proof and/or a distinction between both reaction pathways 5a and 5b might come from the ^{11}B high-resolution NMR spectra, where either two distinct tetrahedral boron species and/or two distinct trigonal boron species could be expected. However, even in the well-resolved TQMAS spectra only single resonances are observed for both types of boron species. We suspect that the respective ^{11}B chemical shift differences between $BO_{4/2}^-$ and $BO_{3/2}F^-$ groups on the one hand, and the $BO_{3/2}$ and the $BO_{2/2}F$ groups on the other, are too small compared to the overall chemical shift distribution caused by other local site geometry variations in the glass. However, both the $^{11}B\{^{19}F\}$ and the $^{19}F\{^{11}B\}$ REDOR data (Figures 4 and 10) signify strong magnetic dipole–dipole interactions between both nuclear species, in support of the mechanisms described by eqs 5a and 5b.

Conclusions

On the basis of a number of complementary solid-state single- and double-resonance NMR experiments, we have developed a model for the structural role of LiF additive in ion-conducting lead borate glasses. LiF is seen to actively participate in the network transformation process contributing to the conversion of three- into four-coordinate boron units, in addition to the formation of volatile BF_3, accounting for the fluorine loss. However, part of the fluoride remains in the dopant role, possibly in the form of small LiF-like cluster domains, which serve as a mobile ion supply. The fact that the fluoride species located in these Li-dominated environments also show a sizable $^{19}F\{^{11}B\}$ REDOR effect, and also the diminished $^7Li-^{19}F$ dipolar interaction strengths in relation to LiF suggest that such domains in these glasses must be quite small. Most probably, the local environment of many of these lithium species is made up of both types of fluoride ions, in addition to some oxide. Fluoride is also seen to contribute to the first coordination sphere of the Pb^{2+} ions, as revealed by the $^{207}Pb\{^{19}F\}$ SEDOR data. The partial integration of F into the network (bonding to boron) may explain the lower ionic mobility seen in Figure 2c for the fluoride ions as compared to the lithium ions. Overall the present work shows the power and potential of advanced solid-state dipolar NMR techniques in elucidating the structural role of the LiF additive in borate glasses.

References and Notes

(1) Ghosh, S.; Ghosh, A. *J. Appl. Phys.* **2005**, *97*, 123525.
(2) Hayashi, A. *J. Ceram. Soc. Jpn.* **2007**, *115*, 110, and references cited therein.
(3) Hayashi, A.; Nakai, M.; Tatsumisago, M.; Minami, T.; Katada, M. *J. Electrochem. Soc.* **2003**, *150*, A582.
(4) Tatsumisago, M. *Solid State Ionics* **2004**, *175*, 13.
(5) Meyer, B.; Borsa, F.; Martin, D. M.; Martin, S. W. *Phys. Rev. B* **2005**, *72*, 144301.
(6) Joo, K. H.; Vinatier, P.; Pecquernard, P.; Levasseur, A.; Sohn, H. J. *Solid State Ionics* **2003**, *160*, 51.
(7) Wang, B.; Szu, S. P.; Greenblatt, M. *J. Non-Cryst. Solids* **1991**, *134*, 249.
(8) Babu, P.; Jaysankar, C. K. *Phys. B* **2001**, *301*, 326.
(9) Kassab, L. R. D.; Courrol, L. C.; Morais, A. S.; Tatumi, S. H.; Wetter, N. U.; Gomes, L. J. *Opt. Soc. Am. B* **2002**, *19*, 2921.
(10) Adams, S.; Swenson, J. *J. Phys.: Condens. Matter* **2005**, *17*, S87.
(11) Swenson, J.; Karlsson, C.; Börjesson, L.; Heenan, R. K. *Phys. Rev. B* **2001**, *64*, 134201.
(12) Chowdari, B. V. R.; Rong, Z. *Solid State Ionics* **1995**, *78*, 133.
(13) Varsamis, C. P. E.; Vegiri, A.; Kamitsos, E. I. *Phys. Rev. B* **2002**, *65*, 104203.
(14) Matsuo, T.; Shibasaki, M.; Katsumata, T. *Solid State Ionics* **2002**, *759*, 154–155.
(15) Eckert, H. *Prog. NMR Spectrosc.* **1992**, *24*, 159.
(16) Böhmer, R.; Jeffrey, K. R.; Vogel, M. *Prog. NMR Spectrosc.* **2007**, *50*, 87.
(17) Estalji, S.; Küchler, R.; Kanert, O.; Bölter, R.; Jain, H.; Ngai, K. L. *J. Phys. IV* **2 1992**, (Colloque C), 159.
(18) Geissberger, A. E.; Bucholtz, F.; Bray, P. J. *J. Non-Cryst. Solids* **1982**, *49*, 117.
(19) Bobe, J. M.; Reau, J. M.; Senegas, J.; Poulain, M. *J. Non-Cryst. Solids* **1997**, *209*, 122.
(20) Kavun, V. Y.; Merkulov, E. B.; Goncharuk, V. K. *Glass Phys. Chem.* **2004**, *30*, 320.
(21) Reau, J. M.; Rossignol, S.; Tanguy, B.; Paris, M. A.; Rojo, J. M.; Sanz, J. *Solid State Ionics* **1995**, *80*, 283.
(22) Rojo, J. M.; Sanz, J.; Reau, J. M.; Tanguy, B. *J. Non-Cryst. Solids* **1990**, *116*, 167.
(23) Rojo, J. M.; Herrero, P.; Sanz, J.; Tanguy, B.; Portier, J.; Reau, J. M. *J. Non-Cryst. Solids* **1992**, *146*, 50.
(24) Minami, T. *J. Non-Cryst. Solids* **1983**, *56*, 15.
(25) Olsen, K. K.; Zwanziger, J. W. *Solid State Nucl. Magn. Reson.* **1995**, *5*, 123.
(26) Olsen, K. K.; Zwanziger, J. W.; Hartmann, P.; Jäger, C. *J. Non-Cryst. Solids* **1997**, *222*, 199.
(27) Swensson, J.; Börjesson, L.; Howells, W. S. *Phys. Scr., T* **1995**, *57*, 117.
(28) Varsamis, C. P. E.; Kamitsos, E. I.; Tatsumisago, M.; Minami, T. *J. Non-Cryst. Solids* **2004**, *93*, 345–346.
(29) Cramer, C.; Price, D. L.; Saboungi, M. L. *J. Phys.: Condens. Matter* **1998**, *10*, 6229.
(30) Müller-Warmuth, W.; Poch, W.; Sielaff, G. *Glastech. Ber.* **1970**, *43*, 5.
(31) Kaplan, D. E.; Hahn, E. L. *J. Phys. Radium* **1958**, *19*, 821.
(32) Gullion, T.; Schaefer, J. *J. Magn. Reson.* **1989**, *81*, 196.
(33) Eckert, H.; Elbers, S.; Epping, J. D.; Janssen, M.; Kalwei, M.; Strojek, W.; Voigt, U. *Top. Curr. Chem.* **2004**, *246*, 195–233.
(34) Zhang, L.; de Araujo, C. C.; Eckert, H. *J. Phys. Chem. B* **2007**, *111*, 10402.
(35) Epping, J. D.; Strojek, W.; Eckert, H. *Phys. Chem. Chem. Phys.* **2005**, *7*, 2384.
(36) Puls, S. P.; Eckert, H. *Phys. Chem. Chem. Phys.* **2007**, *9*, 3992.
(37) Medek, A.; Harwood, J. S.; Frydman, L. *J. Am. Chem. Soc.* **1995**, *117*, 12779.
(38) Amoureux, J. P.; Fernandez, C.; Steuernagel, S. *J. Magn. Reson. A* **1996**, *123*, 116.
(39) Züchner, L.; Chan, J. C. C.; Müller-Warmuth, W.; Eckert, H. *J. Phys. Chem. B* **1998**, *102*, 4495.
(40) Chan, J. C. C.; Eckert, H. *J. Magn. Reson.* **2000**, *147*, 170.
(41) Massiot, D.; Farnan, I.; Gautier, N.; Trumeau, D.; Trokiner, A.; Coutures, J. P. *Solid State Nucl. Magn. Reson.* **1995**, *4*, 241.
(42) Bureau, B.; Silly, G.; Buzàre, J. Y.; Legein, C.; Massiot, D. *Solid State Nucl. Magn. Reson.* **1999**, *14*, 181.
(43) Montagne, L.; Donze, S.; Palavit, G.; Boivin, J. C.; Fayon, F.; Massiot, D.; Grimblot, J.; Gengembre, L. *J. Non-Cryst. Solids* **2001**, *74*, 293–295.
(44) Zhou, D. H.; Hoatson, G. L.; Vold, R. L.; Fayon, F. *Phys. Rev. B* **2004**, *69*, 134104.
(45) Massiot, D.; Fayon, F.; Capron, M.; King, I.; Le Calvè, S.; Alonso, B.; Durand, J. O.; Bujoli, B.; Gan, Z.; Hoatson, G. *Magn. Reson. Chem.* **2002**, *40*, 70.
(46) Macdonald, J. R. *Impedance Spectroscopy—Emphasizing Solid Materials and Systems*; John Wiley & Sons: New York, 1987.
(47) Cole, K. S.; Cole, R. H. *J. Chem. Phys.* **1941**, *9*, 341.
(48) Dyre, J. C. *J. Appl. Phys.* **1988**, *64*, 2456.
(49) Gee, B.; Eckert, H. *J. Phys. Chem.* **1996**, *100*, 3705.
(50) van Vleck, J. H. *Phys. Rev.* **1948**, *74*, 1168.
(51) Bray, P. J.; Leventhal, M.; Hooper, H. O. *Phys. Chem. Glasses* **1963**, *4*, 47.
(52) Gross, U.; Rüdiger, S.; Grimmer, A. R.; Kemnitz, E. *J. Fluorine Chem.* **2002**, *115*, 193.